Du, J., Hao, P., Liu, M., & Scarpa, F. (2020). Multi-cell energy-absorbing structures with hollow columns inspired by the beetle elytra. *Journal of Materials Science*, *55*, 4279-4291. https://doi.org/10.1007/s10853-019-04190-4

Multi-cell energy absorbing structures with hollow columns inspired by the beetle elytra

Jianxun Du[1], Peng Hao[2,3], Mabao Liu[1], Fabrizio Scarpa[4*]

1. State Key Laboratory for Strength and Vibration of Mechanical Structures, School of Aerospace Engineering, Xi'an Jiaotong University, Xi'an 710049, Shaanxi, China
2. School of Mechanical Engineering, Tianjin University, Tianjin 300072, China
3. School of Aeronautic Engineering, Civil Aviation University of China, Tianjin 300300, China
4. Bristol Composites Institute (ACCIS), University of Bristol, Bristol BS8 1TR, UK

Abstract

In this work we propose a new type of thin-walled energy absorbed structure with hollow columns that possesses a design inspired by the beetle elytra. The failure mode of the bionic thin-walled structures is firstly discussed by developing a theoretical model. The energy absorption properties of these bio-inspired multi-call thin-walled structures have been then investigated using nonlinear finite element simulations. The values of the specific energy absorption and the crushing force effectiveness have been evaluated for different structures with parametrized column nested configurations. Dynamic impact simulations of multi-cell tubes with different columns nested modes, wall thickness and impact angles have been performed and the results discussed.

Keywords: beetle elytra; bionic multi-cells tube; thin-walled structure; geometric parameter; energy absorbed material

ORCID iD:

Jianxun Du: https://orcid.org/0000-0003-4572-2755

Peng Hao: https://orcid.org/0000-0002-5239-4991

Mabao Liu: https://orcid.org/0000-0002-8350-8381

Fabrizio Scarpa: https://orcid.org/0000-0002-5470-4834

Corresponding author: Fabrizio Scarpa

E-mail addresses: f.scarpa@bristol.ac.uk (F. Scarpa)

1. Introduction

Thin-walled structures have been recently widely used to design airframe and vehicles components due to their remarkable lightweight performance and energy absorption characteristics [1] [2]. Several attempts have been carried out to investigate thin-walled structures in different loading conditions through experiments [3-4], theoretical studies[5-6] and simulations [7-9]. Aluminum alloys have been extensively used to design thin-walled tubes of various shapes because of their good mechanical properties and relatively low processing costs[10-13]. Wang[14] has discussed the development of different geometric configurations of thin-walled structures based on honeycomb configurations. His work has shown that these lightweight structures feature desirable properties, but also need further experimental and simulation work to complete their characterization under quasi-static and crushing load. The mechanical behavior of thin-walled multi-cell tubes combined within vertex-based hierarchical configurations has also been analyzed from a theoretical and numerical perspective [15-16]. The lateral crushing and energy absorption properties of thin-walled structures under different parameters have also been studied under quasi-static experimental and simulation tests[17-18]. Besides employing aluminum alloy, carbon fiber reinforced plastic (CFRP) has also been adopted to design thin-walled structures[19-21]. Compression experiments of thin-walled CFRP structures have shown that these structural elements are excellent lightweight absorbers. Foam filled thin-walled structures also play an important role in the field of energy absorption due to the mechanical properties of the foam and the interaction between the foam and the confining shell[22-24]. Finite Elements have also been used to compare the mechanical characteristics and energy absorption efficiency of empty and foam filled tubes, with a general satisfactory agreement observed between simulations and experimental results [25-27]. A type of novel thin-walled structure inspired by the topology of the bamboo stem features a peculiar rib shape and number of ribs. This thin-walled structure has shown some very interesting characteristics in terms of energy absorption under axial crushing[28-29]. Multi-objective optimization has also been used to design parametric configurations of this type of thin-walled structure[30-31].

Although the design and investigation of the mechanics of thin-walled structures has been quite popular in recent years, a relatively less explored field is the development of bionic lightweight structures. From the 4D printing of structural elements designed from bio-inspired

botanical systems[32] to the design of micro air vehicles biomimicking the fruit fly[33], nature has had a profound impact on the development of modern science and technology. In addition to theoretical and experimental activities[34], finite element simulation has been widely used to explore the mechanical characteristics of bionic structures [35-38]. The work of Naleway et al has classified eight topologies of structures inspired by biological materials: the cellular, fibrous, helical, tubular, gradient, suture, overlapping and layered configurations[39]. The beetle's elytra protect its hindwing and body from potential outside damage by limiting the transfer of external loads. The hollow honeycomb-like thin-walled structure exists in the internal structure of the elytra, in which there are circular hollow columns (Fig. 1)[40-41]. Although internal structures of beetle elytra possess unique internal configurations, little work [42-43] has been performed to develop thin-walled structures inspired by beetle elytra for energy absorption structural elements. This study focuses on new types of energy absorbing structures that possess configurations inspired by the beetle elytra. The energy absorption mechanism of these bionic thin-walled structures is first discussed theoretically, and then further investigated by numerical simulations representing axial impact loading. The values of the specific energy absorptions and crushing forces effectiveness of all the new thin-walled structures have been calculated, also considering different column nested methods. Dynamic impact simulations of multi-cell tubes with different nested columns modes, wall thicknesses and impact angles have been also performed and discussed to offer a broader view of the general impact absorption properties of these bionic structures.

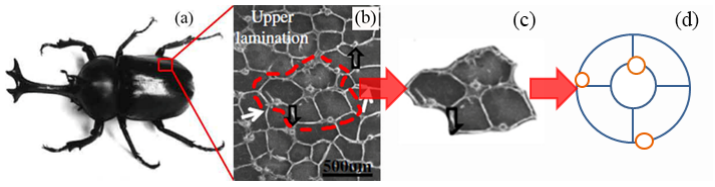

Fig.1 Multi-cell thin-walled tube with tubular inspired by internal structure of beetle elytra: (a) beetle; (b) cross-sectional internal structure of beetle elytra [40]; (c) the multi-cell unit (d) bionic multi-cell thin-walled structure.

2. Multi-cell configurations and Finite Element Models

An effective way to benchmark the energy absorption performance of different structural elements is to use appropriate metrics. The two most important indicators in crashworthiness and energy absorption performance of structures are the specific energy absorption and the crash load

coefficient [44]. Specific energy absorption (SEA) is used to quantify the energy absorbed by the structure per unit mass, and it is defined as the ration between the total energy (EA) absorbed to the total mass structure (M):

$$\mathrm{SEA} = \frac{\mathrm{EA}}{\mathrm{M}} \tag{1}$$

The crash load efficiency (CLE) denotes the ratio of the mean crushing force (MCF) to the peak force (MIF):

$$\mathrm{CLE} = \frac{\mathrm{MCF}}{\mathrm{MIF}} \times 100\% \tag{2}$$

The bionic multi-cell thin-walled structure proposed in this work is shown in Fig. 2, and it can be divided into four types according to the configuration of the baseline structures. A visual inspection of Fig. 1 makes it clear that the cellular configuration of the elytra is composed by a hierarchical assembly of larger and smaller tubes; the biomimetic cellular topology investigated in this work follows similar patterns of tubes with different diameters. All the cross-sections of the inner tubes are circular and fixed in size. The outer tubes are divided into circular, and quadrilateral, hexagonal and octagonal regular hollow prisms. The inner tube and the outer tube are connected by thin-walled (shear wall) structures. We evaluate in this work five different assemblies of hollow columns (Fig.2). To benchmark the energy absorption of these different structures, we have considered a fixed total height (200 mm), a constant diameter (50 mm) of the inner tube, and the wall thickness *t* as a design variable.

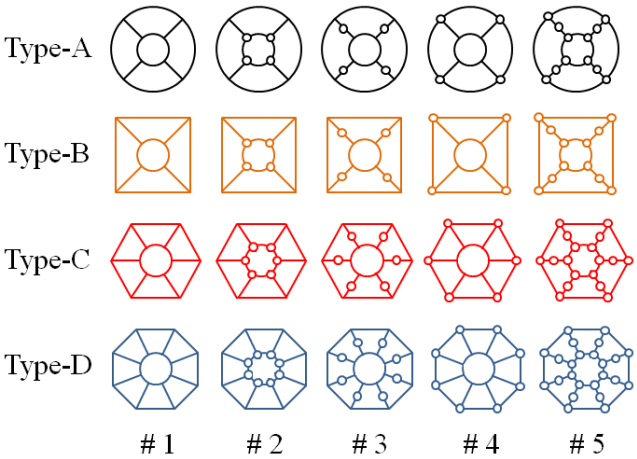

Fig. 2. Cross-sectional configurations of the bionic multi-cells tubular thin-walled structures investigated in this work.

Aluminum alloy AA6063 T6 is adopted here as the material composing all the bionic

thin-walled structures. The density of the aluminum alloy AA6063 T6 2.7×10^3 kg/m^3, the Poisson's ratio is 0.3, initial yield stress is 162 MPa, and the Young's modulus is 68.2 GPa [45]. The bionic thin-walled structure is modeled using shell elements (61409 nodes) from the preprocessing Hypermesh 12.0, with the material parameters imported in LS-DYNA 971. Aluminum alloy AA6063 T6 shows small strain rate sensitivity[46].

The baseline Finite element model with boundary conditions used in this work is shown in Fig.3. The bottom of the thin-walled tube is fixed to the bottom plate. To simplify the calculations and save computing time the impactor is represented as a rigid body. The impactor has an initial velocity v of 10 m/s and mass m of 500 kg. Automatic contact setup is adopted to simulate the contact occurring between the tubular walls during crushing. A point-to-surface model is employed to describe the contact happening between the multi-cell thin-walled structure and the rigid wall. The coefficients of dynamic and static frictions are 0.15 and 0.13, respectively[47]. Material failure of the aluminum alloy tube in this work is neglected [48].

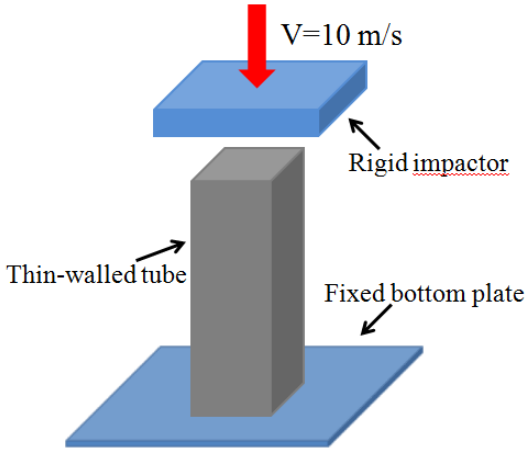

Fig. 3. Boundary conditions used for the finite element model simulations.

The CATIA V5R20 software is used to build the solid model of multi-cell thin-walled structures, while Hypermesh is adopted as the pre-processor to set the boundary conditions during the impact crushing, including material properties, constraint conditions and rigid wall. The explicit nonlinear finite element software LS-DYNA is used to calculate the energy absorption characteristic of thin-walled structure. For a convergence study, five different mesh densities ranging from 1.5 mm to 3.5 mm of dimensions for the shell elements have been evaluated. The curves representing the crushing force of the thin-walled tubes versus top displacement for the five

mesh densities are shown in Fig. 4. Meshes with element sizes of 1.5 mm and 2.0 mm show very little discrepancy and both possess sufficient accuracy for the estimation of the crushing force. The average CPU times for these above simulations are 3.5 hours. To reduce the computation times, a mesh size of 2.0 mm is adopted for the finite element simulations in this work.

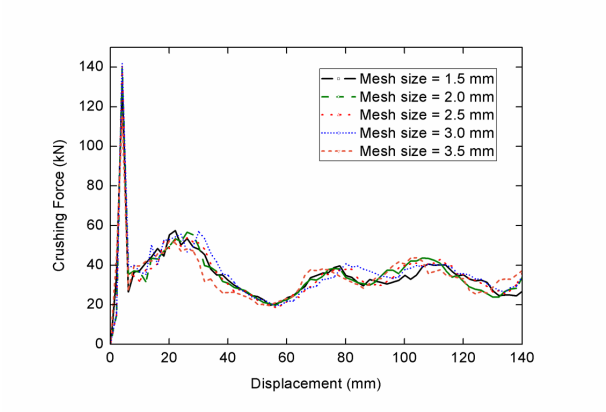

Fig. 4. Crushing force versus displacement of multi-cells tubes with different mesh sizes.

To benchmark the model, we have reproduced the experimental results obtained by Lee et al. [49] on thin-walled square tubes under crushing. The experimental tube is made of Al 6063 alloy. The length and weight of the tube are 200 mm and 40 kg, respectively. The velocity of the impactor in Lee et al's work is 7.02 m/s. The numerical results obtained by our model reproducing the experimental conditions of [49] are compared with the test ones in Figs. 5 and 6. Fig. 5 shows that the numerical crushing force versus displacement agrees well with the one from the experiments, in particular in terms of peak force and sequence of the collapsing modes. In addition, the global crushing mode predicted by the numerical simulation matches well with the experimental one (Fig. 6). One could therefore argue that the finite element methodology adopted in this work is able to calculate the energy absorption properties of thin-walled structures with a good fidelity.

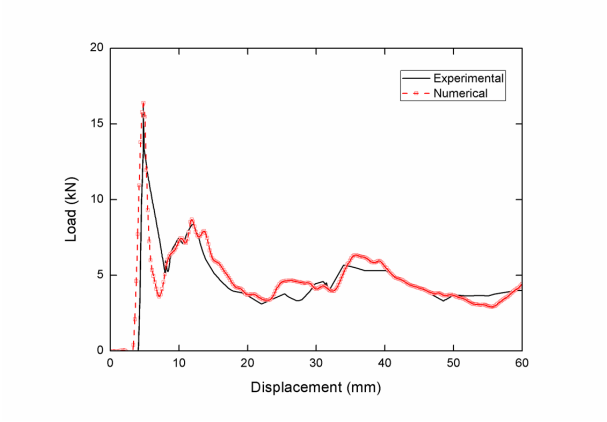

Fig. 5. Comparison of the force versus displacement between experimental and numerical results.

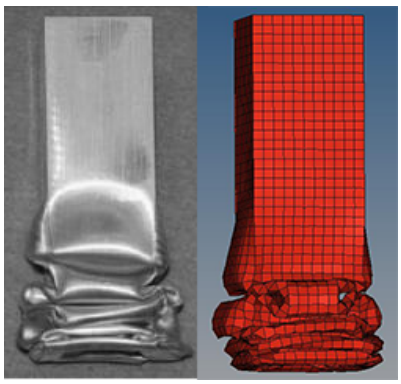

Fig. 6. Comparison of the deformation patterns of the thin-walled square hollow tube given by the experimental and numerical results.

3. Theoretical study

The theoretical model developed to predict the mechanical properties of thin-walled structures under impact loading is based on the adoption of the *Super Folding Element* method [50-51]. Following this approach, the mean (average) crushing force P_m can be expressed by

$$P_m = 13.06\sigma_0 b^{\frac{1}{3}} t^{\frac{5}{3}} \tag{3}$$

Where σ_0 is the flow stress, t is the thickness of the thin-walled structure and b is the width of the cross-section. When the thin-walled structure is deformed under an impact load, a wave propagation is triggered. The half wavelength can be calculated as:

$$H = 1.276 b^{\frac{3}{2}} t^{\frac{1}{3}} \tag{4}$$

The material's flow stress can be considered as equivalent stress [49]

$$\sigma_0 = \sqrt{\frac{\sigma_y \sigma_u}{1+n}} \tag{5}$$

Where σ_y and σ_u are the yield and ultimate stresses, respectively. The index n is the exponent

of the power law.

The deformation mechanisms occurring during the crushing can be represented into deformation elements and bending lines. The equilibrium for one wavelength in the folding can be written as

$$\mathrm{P_m} \times 2\mathrm{H} = \mathrm{U_b} + \mathrm{U_m} \tag{6}$$

Where U_b and U_m denote, respectively, bending the energy and the membrane energy associated to one wavelength. The membrane energy U_m can be expressed as:

$$\mathrm{U_m} = \int_S \sigma_0 \mathrm{t} ds = \frac{1}{2}\sigma_0 \mathrm{t}\mathrm{H}^2 = 2\mathrm{M_0}\frac{\mathrm{H}^2}{\mathrm{t}} \tag{7}$$

Where $\mathrm{M} = \frac{1}{4}\sigma_0 \mathrm{t}^2$

The bending energy U_b can be calculated as:

$$\mathrm{U_b} = \sum_{i=1}^{3} \mathrm{M_0}\theta_i \mathrm{c} \tag{8}$$

Where θ_i denotes the rotation angle of the i^{th} hinge line. Because the angles θ_i for all the hinge lines are $\frac{\pi}{2}$, π and $\frac{\pi}{2}$, the term U_b can be calculated as:

$$\mathrm{U_b} = 2\pi \mathrm{M_0 c} \tag{9}$$

The crushing force P_m can be therefore expressed as:

$$\frac{\mathrm{P_m}}{\mathrm{M_0}} = \left(\frac{\mathrm{H}}{\mathrm{t}} + \pi\frac{\mathrm{c}}{\mathrm{H}}\right) \tag{10}$$

Compared to a theoretical wavelength, the effective crushing distance is however reduced [48]. Eq. (8) could be modified as:

$$\frac{\mathrm{P_m}}{\mathrm{M_0}} = \frac{4}{3}\left(\frac{\mathrm{H}}{\mathrm{t}} + \pi\frac{\mathrm{c}}{\mathrm{H}}\right) \tag{11}$$

If *N* contributing flanges are present in a thin-walled structure the crushing force P_m can be expressed as:

$$\frac{\mathrm{P_m}}{\mathrm{M_0}} = \frac{4}{3}\sum_{i=1}^{N}\left(\frac{\mathrm{NH}}{\mathrm{t}} + \frac{\pi \mathrm{l}}{\mathrm{H}}\right) \tag{12}$$

Where *l* denotes the total length of the thin walls of the cross-section. Further mathematical manipulation leads to the force P_m being finally expressed as:

$$\mathrm{P_m} = \frac{2}{3}\sigma_0 \mathrm{t}\sqrt{\pi \mathrm{NA}} \tag{13}$$

Where *A* is the cross-sectional area of material. As examples of the application of Eq. (13), the mean crushing force associated to the configurations C-#1 and type D-#1 can be calculated as:

$$\mathrm{P_m}\,(\mathrm{C\#1}) = 172.96\sigma_0 \mathrm{t}^{\frac{3}{2}} \text{ (N=36, A=595.46t)} \tag{14}$$

$$P_m\,(D\#1) = 209.63\sigma_0 t^{\frac{3}{2}} \quad (15)$$

4. Numerical study

4.1. Effect of column nested method

Table 1. Data related to every configuration evaluated with different column nested methods

No.	Structure	Mass(kg)	PCF(kN)	P_m(kN)	EA(kJ)	SEA(kJ/kg)	CFE(%)
1	Type A *	0.1269	70.86	22.38	2.52	19.86	31.58
2	Type A #1	0.2295	123.61	49.34	5.78	25.19	39.92
3	Type A #2	0.2538	136.26	65.55	7.65	30.14	48.11
4	Type A #3	0.2619	140.09	70.15	8.24	31.46	50.07
5	Type A #4	0.2565	135.25	66.68	7.68	29.94	49.30
6	Type A #5	0.3132	161.96	99.78	11.58	36.97	61.61
7	Type B *	0.1134	59.80	15.27	1.74	15.34	25.54
8	Type B #1	0.2106	109.86	42.56	4.90	23.27	38.74
9	Type B #2	0.2376	123.34	57.86	6.67	28.07	46.91
10	Type B #3	0.2457	127.57	65.66	7.59	30.89	51.47
11	Type B #4	0.2430	127.73	61.31	7.09	29.18	48.00
12	Type B #5	0.2997	156.15	94.29	10.98	36.64	60.38
13	Type C *	0.1215	62.21	17.56	1.99	16.38	28.23
14	Type C #1	0.2430	126.71	52.49	6.09	25.06	41.43
15	Type C #2	0.2808	145.43	75.52	8.76	31.20	51.93
16	Type C #3	0.2916	152.38	84.78	9.85	33.78	55.64
17	Type C #4	0.2808	147.33	79.07	9.23	32.87	53.67
18	Type C #5	0.3672	189.28	126.74	14.86	40.47	66.96
19	Type D *	0.1242	63.46	18.04	2.07	16.67	28.43
20	Type D #1	0.2646	138.91	58.22	6.72	25.40	41.91
21	Type D #2	0.3132	163.02	90.21	10.47	33.43	55.34
22	Type D #3	0.3294	172.14	100.33	11.60	35.22	58.28
23	Type D #4	0.3159	166.08	97.54	11.33	35.87	58.73
24	Type D #5	0.4320	220.98	161.52	19.14	44.31	73.09

* configurations with no filling material or nested mode.

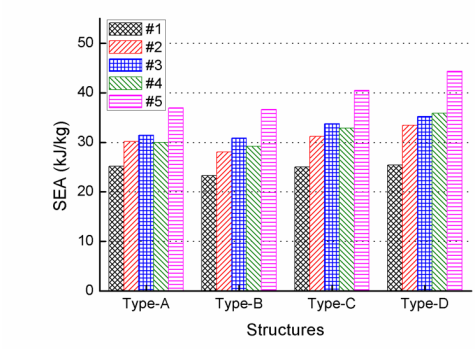

(a)

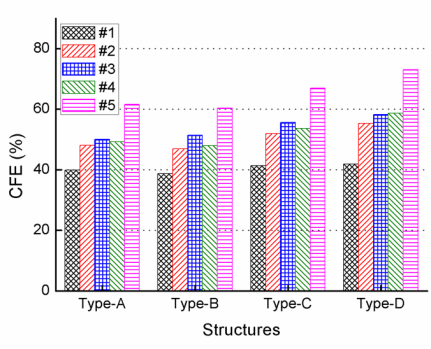

(b)

Fig. 7. Crashworthiness data of the bionic thin-walled structures with different cross-sectional configurations and nested style: (a) SEA values; (b) CFE values.

Tab.1 shows the data of energy absorption properties of all type structures with different nested column. Apparently, the configurations without nested mode show some poor energy absorption capabilities compared to the structure with the nested topology. Fig.7 shows the specific energy absorption and crushing force efficiency of four configurations with different nested modes. Configuration #5 (which corresponds to the largest tube nested) has the highest value of specific energy absorption among the same type of structures. The values of specific energy absorptions for configurations with nested tubes #2，#3 and #4 in the four types of structures are however similar. For the A, B and C types the specific energy absorption with the internal architecture #3 is slightly higher than those related to #2 and #4. The internal nested tubes architecture #1 has the lowest specific energy absorption value and it is significantly lower than other structures with different internal architectures. The distribution of the crushing efficiency of the various structures is also quite similar to the one of the SEA values. The crushing efficiency of the configurations with the internal architecture #5 is the highest, with the internal arrangement #1 providing the lowest CLE.

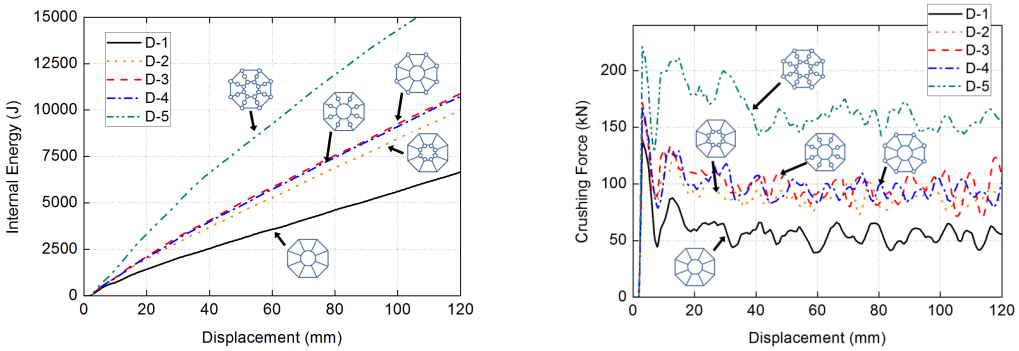

Fig.8. Crushing performance of the bionic structures with octagonal cross-sections with different columns arrangements: (a) absorbed energy versus displacement; (b) crushing force versus displacement.

The energy absorption and crushing force versus displacement diagrams of the regular octagonal structures for the five types of internal colums arrangements are shown in Fig.8. From Fig.8 (a), it can be seen that the trends of energy absorption of octagonal structure with different nested modes of column are relatively stable. At the beginning of collision, the energy absorption curve of the structure with #5 nested method appeared obviously increase, and always higher than

other curves in the whole process, while the energy absorption curve of #1 structure is lower than other curves in the whole process. The trend of other three curves are relatively similar, and the energy absorption curve of structure with #2 nested method is slightly high than that of other structures. Fig.8 (b) is the crushing force displacement history diagram of octagonal structures filled with various hollow columns. It can be seen from the figure that all structures presents multiple peaks during the impact loading, which indicates that many folds occurred during the collision and the energy absorbed by structure is more sufficient. The energy absorption curve shows a satisfactory consistent result compared to that of Fig.8 (a) that the crushing force curve of structure with #5 nested method is higher than that of other structures, while the crushing force curve of structure with #1 nested method is significantly lower than that of other structures.

4.2. Effect of the outer wall configurations

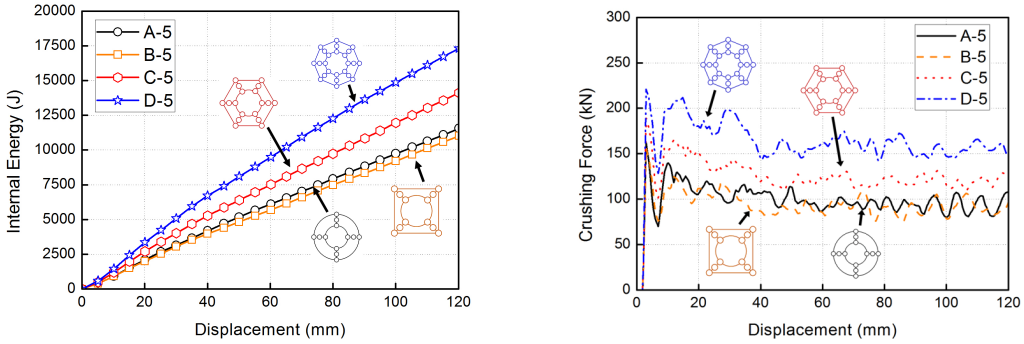

(a) (b)

Fig.9. Crushing performance of different cross-sections of bionic structures with columns:(a) absorbed energy versus displacement curves; (b) crushing force versus displacement curves.

The energy absorption curves and crushing force displacement history diagrams of four kinds of bionic thin-walled structures filled with #5 nested mode was shown in Fig.9. Fig.9 (a) shows that the trends of energy absorption curves of the structures are relatively stable. The energy absorbed by octagonal structure are highest between the other three kinds of structures, followed by the hexagonal structure. The energy absorption curves of circular and quadrilateral structures are the lowest and the energy absorption values are close to each other. It can be seen from the Fig.9 (b) that the crushing force versus displacement curves of structures with #5 column nested mode. The curve of octagonal structure is higher than that of other structures, the curve of hexagon is at the second highest position, and the curves of the other two structures are relatively

close. This is consistent with the trend of energy absorption of each structure in Fig.9(a).

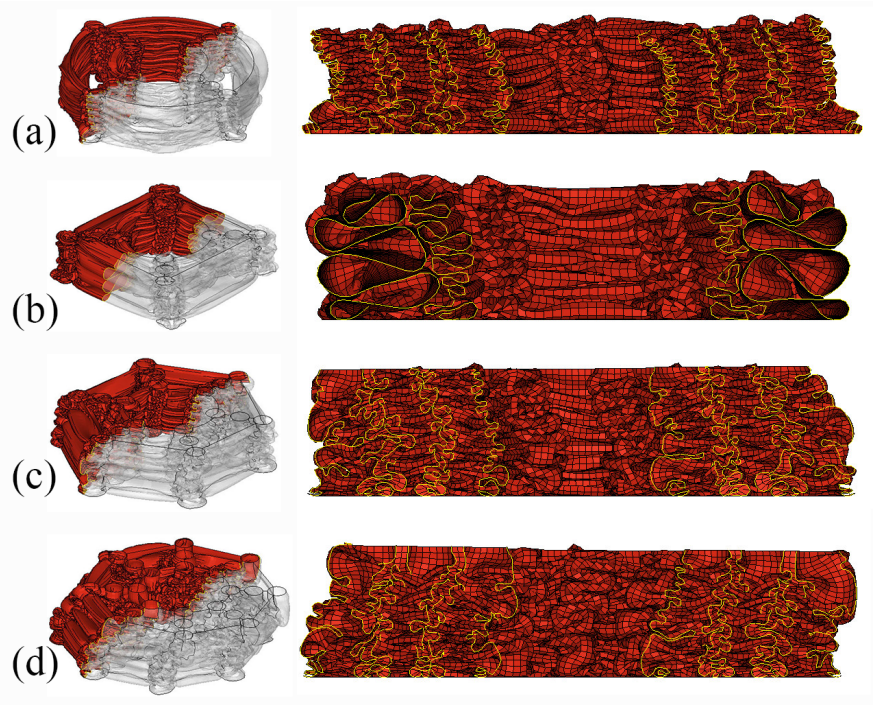

Fig.10. Cross-sectional deformation diagrams of different structures under impact loading: (a) circle; (b) quadrangle; (c) hexagon; (d) octagon.

The cross-sectional diagram of four types of structures with #5 column nested mode and crushing displacement of 120 mm are shown in Fig.10. The left column represents the cross-section of the structure under crushing force, which is set as the white transparent part in the right and the red part in the left. The yellow curve in the right column represents the irregular shape of the thin-walled configuration formed by folds under impact load. As it can be observed from the graph, the yellow curve in the cross-section of circular structure assumes a more symmetrical shape than other configurations, and the folds of the hexagonal and octagonal cross-sections have a more chaotic distribution.

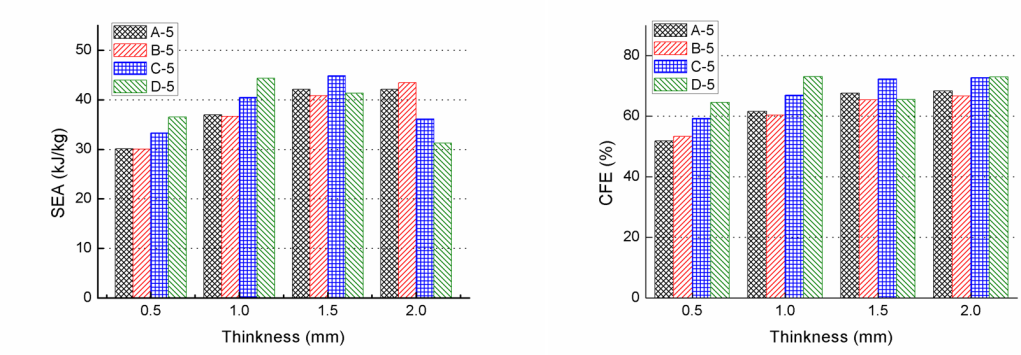

(a) (b)

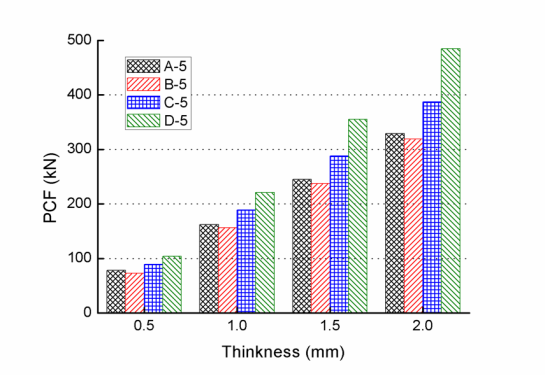

(c)

Fig.11. Crashworthiness data of the bionic thin-walled structures with different thickness: (a) SEA values; (b) CFE values; (c) PCF values.

The specific energy absorption, crushing efficiency and maximum crushing force peak of the four types of structures with the #5 column nested type and different thicknesses are shown in Fig.11. The behavior of the energy absorbed by the structures with a wall thickness of 0.5 mm and 1.0 mm are all ralatively similar (Fig. 11(b)); the order of the structures with decreasing energy absorption characteristics is the octagonal, hexagonal, circular and quadrilateral. When the wall thinkness is 1.5 mm the above sequence of configurations is changed (hexagonal, circular, octagonal and quadrilateral). When the wall thickness is 2.0mm, the SEA value of the octagonal structure is significantly reduced, followed by the one of the hexagonal configuration. As shown in Fig.11(b), the distribution of the SEA with wall thickness of 0.5 mm, 1.0 mm and 1.5 mm is very similar to the one shown in Fig. 11(a). When the wall thickness is 2.0 mm the specific energy absorptions of octagonal and hexagonal structures are highest, while SEA values belonging to circular and quadrilateral structures are the the lowest for all the cases considered. The maximum crushing force of the quadrilateral structure is the lowest for all the different wall thickness values considered, followed then by the circular configuration (Fig. 11(c)). The peak crushing force value of the octagonal structure with different wall thickness is the highest, followed by the one of the hexagonal structure. With the increase of the wall thickness the difference between the quadrilateral and circular configurations is increasing. For a 0.5 mm displacement the difference of the maximum peak values between the octagonal and the quadrilateral structures is no more than 30 kN. For a 2.0 mm displacement that difference is however close to 200 kN. The variation of the wall thickness has a significant impact on the SEA values, maximum crushing

force and CFE values for all the different configurations of the bionic thin-walled structures considered in this work.

4.3. Effect of the impact angle

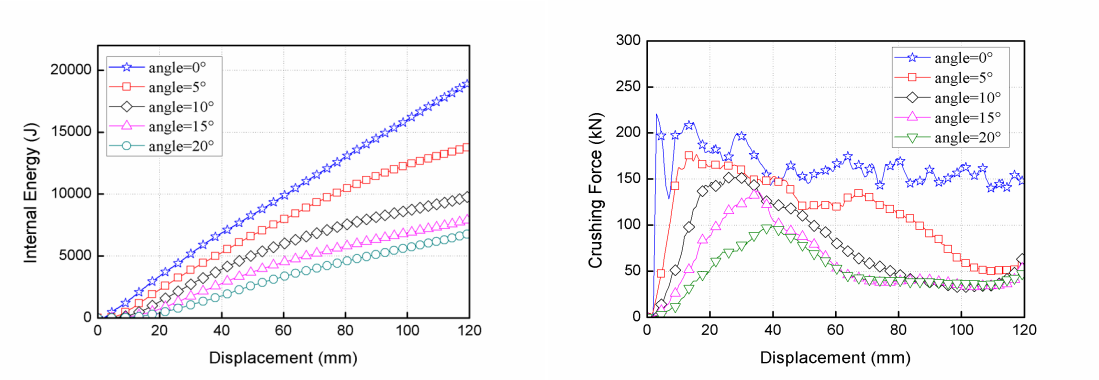

(a) (b)

Fig.12. Crushing performance of the bionic structures with different impact angles:(a) absorbed energy versus displacement curves; (b) crushing force versus displacement curves.

The energy absorption characteristics of the octagonal cross-section thin-walled structures with different impact angles are shown in Fig.12. The inclination angle is varied from 0º to 20º with a step of 5 degrees by changing the angle of the rigid plate. The simulations are carried out with normal displacements from 0 mm to 120 mm. The energy absorption of thin-walled structure in different inclination angles increases steadily during the impact process (Fig. 12(b)). The growth rate of the structure is stable at different impact angles, and the energy absorption of the configurations decreases with the increase of the impact angles when crushing from 0 mm to 60 mm. A softening of the growth rate is observed for angles between 5 and 15 degrees. Although the trends related to the energy absorption of the configuration with the five values of inclination angles are different from each other, the distribution of the total energy absorbed follows a constant pattern. At 120 mm of displacement the energy absorbed by the structures between 0 and 5 degrees are 19kJ and 14kJ, respectively; when the angles are increased to 10º and 20º the energies absorbed are now between 5 kJ and 10 kJ. Overall, the energy absorbed by the structure is reduced by a factor of four times when the inclination angle changes from 0º to 20º. The softening of the rate of increase of the energy absorbed versus the displacement is accelerated for the highest impact angles.

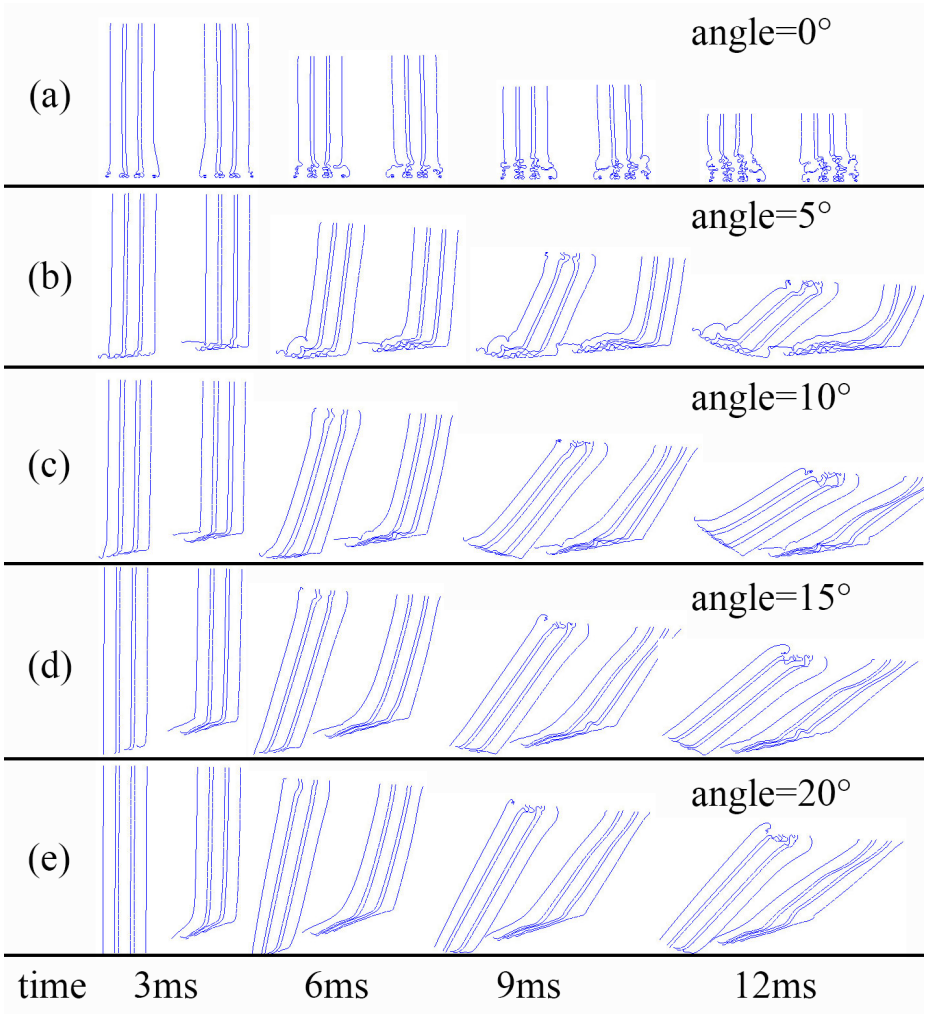

Fig.13. Time histories of the cross-sectional deformation of the bionic structures at different impact angles: (a)0°; (b) 5°; (c) 10°; (d) 15°; (e) 20°.

Fig.12(b) shows the crushing force-displacement curves of the structures at different impact angles. The first peak happens at later stages with the increase of the impact angle; the first peak with impact at 0 degrees occurs almost at the beginning, while for a 20º impact the same peak occurs at 40 mm of displacement. The intensity of the peak also decreases gradually with the increase of the impact angle, from about 230 kN at 0 degrees to 100 kN at 20º. With the 0º impact a series of multiple peaks is present, and that shows that the deformation of the structure is more effective and the impact energy is better absorbed better than in the other impact angle cases. For the impact angle of 5 degrees one can observe that the deformation of structure is less pronounced after the first peak, and the energy absorbed has a significant decline. In that particular case almost no fluctuations are evident, and that is a sign that the structure almost no longer produces deformations and loses the ability to absorb energy.

The patterns of the deformations of the cross-sections of the structures at different inclination angles and at different instants during the impact (3ms, 6ms, 9ms and 12ms) are shown in Fig.13. When the impact angle is 0 degrees the cross section of the thin-walled structure is obviously folded due to the presence of impact loads with increasing crushing displacements. This shows that the structure absorbs a significant portion of impact energy through deformation. When the inclination angle is 5° both the number and the amplitude of the folds are reduced, and the energy absorption performance of the structures is weakened. When the inclination angle is between 10° and 20° the deformation of the structure is reduced and the deterioration of the energy absorption characteristics becomes more and more obvious with the increase of the inclination angle.

5. Conclusion

In this paper, a type of multi-cell thin-walled energy absorbing structure inspired by the internal structure of the beetle elytra has been proposed. A super folding element method has also been developed to investigate the mechanical properties of these thin-walled structures under impact and their mode of energy absorption. The validity of the method has been verified by comparing against experimental results and finite element simulations of different mesh sizes. The specific energy absorption and crushing force effectiveness for all the structures considered in this work (and made by aluminum alloy) were calculated by using nonlinear finite element models in LS-DYNA. The following main conclusions that can be ascertained from this work are:

1. The energy absorption behaviour of the nested columns with hexagonal configuration with different nested modes of columns is fairly constant across the different geometries. At the beginning of impact the energy absorption curve of the topology #5 is always larger than the one of the other structures at the same instant of loading. All the hexagonal structures feature multiple peaks during the impact that indicate the presence of several folds and an adequate energy absorbtion capability.

2. The specific energy absorption, crushing efficiency and maximum crushing force peak of the four types of structures with #5 column nested configuration and different wall thickness have show some common patterns. The energy absorbed by the structures with the wall thickness between 0.5 mm and 1.0 mm is ralatively similar. When the wall thickness is 1.5 mm the highest absorbed energy is the one related to the hexagonal configuration, followed by the circular,

octagonal and quadrilateral ones. When wall thickness is 2.0 mm, the specific energy absorption values of the octagonal and hexagonal structures are the highest, while the SEA values for circular and quadrilateral configuratios are the lowest. The maximum crushing force of the quadrilateral structure is the lowest, whichever thickness value is considered. The octagonal structure features the highest peak crushing force. With the increase of thickness, the difference between the quadrilateral and circular configurations is increasing. The variation of the wall thickness plays an important role on determining the SEA, maximum crushing force and CFE values.

3. The inclination angle has a significant impact on the energy absorption properties of bionic thin-walled structures. When the configuration is subjected to axial impact loading, all the structures developed in this work show a satisfactory performance. When the impact angle gradually increases from 0 to 5 degrees the rate of the energy absorption versus crushing displacement is lower; with further increases of the impact angle the decrease of the same rate accelerates rapidly.

The bionic thin-walled configurations proposed in this work show some promise as high-performance energy absorbers. The beetle elytra is a source of bioinspiration for mechanical designers, and this work proposes a contribution to the biomimicking of this interesting biological configuration for high-end mechanical applications.

Acknowledgments

This work was supported by the Fundamental Research Funds for the Central Universities (Nos. xjh012019033 and 3122018D041). The authors would like to thank the Aviation Science Foundation (No.201647003) and the Key R&D Plan of Shaanxi Province (No.2018ZDCXL-GY-03-01).

Conflict of interest

The authors declare that they have no conflict of interest.

References:

[1] He Q, Ma D, Zhang Z.Yao L (2015) Mean compressive stress constitutive equation and crashworthiness optimization design of three novel honeycombs under axial compression, Int J Mech Sci 99:274-287.

[2] Rouzegar J, Assaee H, Niknejad A.Elahi S A (2015) Geometrical discontinuities effects on lateral crushing and energy absorption of tubular structures, Mater Design 65:343-359.
[3] Zohrabi M, Niknejad A.Ziaee S (2015) A novel method for enhancing energy absorption capability by thin-walled sections during the flattening process, Thin Wall Struct 97:140-153.
[4] Luo X, Xu J, Zhu J, Gao Y, Nie L.Li W (2015) A new method to investigate the energy absorption characteristics of thin-walled metal circular tube using finite element analysis, Thin Wall Struct 95:24-30.
[5] Ali M, Ohioma E, Kraft F.Alam K (2015) Theoretical, numerical, and experimental study of dynamic axial crushing of thin walled pentagon and cross-shape tubes, Thin Wall Struct 94:253-272.
[6] Elahi S A.Forouzan M R (2019) Increasing the chatter instability speed limit in cold strip rolling using wavy layered composite plates as a damper, Thin Wall Struct 137:19-28.
[7] Rabiee A.Ghasemnejad H (2019) Lightweight design to improve crushing behaviour of multi-stitched composite tubular structures under impact loading, Thin Wall Struct 135:109-122.
[8] Zhang L, Bai Z.Bai F (2018) Crashworthiness design for bio-inspired multi-cell tubes with quadrilateral, hexagonal and octagonal sections, Thin Wall Struct 122:42-51.
[9] Zhou X, Cheng G, Liu J, Yang Y.Chen Y F (2019) Shear transfer behavior at the circular tubed column-steel beam interface, Thin Wall Struct 137:40-52.
[10] Xu F (2015) Enhancing material efficiency of energy absorbers through graded thickness structures, Thin Wall Struct 97:250-265.
[11] Xiang Y, Yu T.Yang L (2016) Comparative analysis of energy absorption capacity of polygonal tubes, multi-cell tubes and honeycombs by utilizing key performance indicators, Mater Design 89:689-696.
[12] Fang J, Gao Y, Sun G, Zheng G.Li Q (2015) Dynamic crashing behavior of new extrudable multi-cell tubes with a functionally graded thickness, Int J Mech Sci 103:63-73.
[13] Wu S, Zheng G, Sun G, Liu Q, Li G.Li Q (2016) On design of multi-cell thin-wall structures for crashworthiness, Int J Impact Eng 88:102-117.
[14] Wang Z (2019) Recent advances in novel metallic honeycomb structure, Composites Part B: Engineering 166:731-741.
[15] Wang Z.Liu J (2019) Numerical and theoretical analysis of honeycomb structure filled with circular aluminum tubes subjected to axial compression, Composites Part B: Engineering 165:626-635.
[16] Wang Z, Li Z, Shi C.Zhou W (2019) Mechanical performance of vertex-based hierarchical vs square thin-walled multi-cell structure, Thin Wall Struct 134: 102-110.
[17] A P K (2019) Influence of plain end-cap on the energy absorption characteristics of cylindrical tubular structures for lateral impact vehicle collisions, Thin Wall Struct 138:32-45.
[18] Huang Z.Zhang X (2019) Three-point bending of thin-walled rectangular section tubes with indentation mode, Thin Wall Struct 137:231-250.
[19] Liu Q, Ou Z, Mo Z, Li Q.Qu D (2015) Experimental investigation into dynamic axial impact responses of double hat shaped CFRP tubes, Composites Part B: Engineering 79:494-504.
[20] Boria S, Obradovic J.Belingardi G (2015) Experimental and numerical investigations of the impact behaviour of composite frontal crash structures, Composites Part B: Engineering 79:20-27.
[21] Li W, An X, Zheng Q, Yang F.Fan H (2019) Hierarchical design, manufacture and crushing behaviors of CFRP tubular energy absorbers, Thin Wall Struct 140:416-425.
[22] Meguid S A, Yang F.Verberne P (2015) Progressive collapse of foam-filled conical frustum using kinematically admissible mechanism, Int J Impact Eng 82:25-35.

[23] Baroutaji A, Gilchrist M D, Smyth D.Olabi A G (2015) Analysis and optimization of sandwich tubes energy absorbers under lateral loading, Int J Impact Eng 82:74-88.
[24] Djamaluddin F, Abdullah S, Ariffin A K.Nopiah Z M (2015) Non-linear finite element analysis of bitubal circular tubes for progressive and bending collapses, Int J Mech Sci 99:228-236.
[25] Ehinger D, Krüger L, Martin U, Weigelt C.Aneziris C G (2015) Buckling and crush resistance of high-density TRIP-steel and TRIP-matrix composite honeycombs to out-of-plane compressive load, Int J Solids Struct 66:207-217.
[26] Hou S, Liu T, Zhang Z, Han X.Li Q (2015) How does negative Poisson’s ratio of foam filler affect crashworthiness? Mater Design 82:247-259.
[27] Azarakhsh S, Rahi A, Ghamarian A.Motamedi H (2015) Axial crushing analysis of empty and foam-filled brass bitubular cylinder tubes, Thin Wall Struct 95:60-72.
[28] Fu J, Liu Q, Liufu K, Deng Y, Fang J.Li Q (2019) Design of bionic-bamboo thin-walled structures for energy absorption, Thin Wall Struct 135:400-413.
[29] Hu D, Wang Y, Song B, Dang L.Zhang Z (2019) Energy-absorption characteristics of a bionic honeycomb tubular filling structure inspired by bamboo under axial crushing, Compos Part B-Eng 162: 21-32.
[30] Yong Z, Xiang X, Jin W, Chen T.Wang C H (2018) Crushing analysis for novel bio-inspired hierarchical circular structures subjected to axial load, Int Mech Sci 140:407-431
[31] Tsang H H.Raza S (2018) Impact Energy Absorption of Bio-inspired Tubular Sections with Structural Hierarchy, Compos Struct 195: 199-210
[32] A. Sydney Gladman E A M R.And Jennifer A. Lewis (2016) 4Biomimetic 4D printing, Nat Mater
[33] Biswal S, Mignolet M.Rodriguez A A (2019) Modeling and control of flapping wing micro aerial vehicles, Bioinspir Biomim 14:026004.
[34] Collins S H, Wiggin M B.Sawicki G S (2015) Reducing the energy cost of human walking using an unpowered exoskeleton, Nature 522:212-215.
[35] Hao P.Du J (2018) Mechanical properties of bio-mimetic energy-absorbing materials under impact loading, J Mater Sci 53:3189-3197.
[36] Hao P.Du J (2018) Energy absorption characteristics of bio-inspired honeycomb column thinwalled structure under impact loading, J Mech Behav Biomed 301-308.
[37] Xiang J.Du J (2017) Energy absorption characteristics of bio-inspired honeycomb structure under axial impact loading, Materials Science and Engineering: A 696:283-289.
[38] Xiang J, Du J, Li D.Scarpa F (2017) Numerical analysis of the impact resistance in aluminum alloy bi-tubular thin-walled structures designs inspired by beetle elytra, J Mater Sci 52:13247-13260.
[39] Naleway S E, Porter M M, Mckittrick J.Meyers M A (2015) Structural Design Elements in Biological Materials: Application to Bioinspiration, Adv Mater 27:5455-5476.
[40] Chen J, Zhang X, Okabe Y, Saito K, Guo Z.Pan L (2017) The deformation mode and strengthening mechanism of compression in the beetle elytron plate, Mater Design 131:481-486.
[41] Chen J, He C, Gu C, Liu J, Mi C.Guo S (2014) Compressive and flexural properties of biomimetic integrated honeycomb plates, Mater Design 64:214-220.
[42] Xu M, Pan L, Chen J, Zhang X, Yu X (2019) The flexural properties of end-trabecular beetle elytron plates and their flexural failure mechanism, J Mater Sci 54:8414-8425.
[43] Yu X, Pan L, Chen J, Zhang X, Wei P (2019) Experimental and numerical study on the energy absorption abilities of trabecular-honeycomb biomimetic structures inspired by beetle elytra, J Mater Sci 54:2193-2204.

[44] Audysho R, Smith R.Altenhof W (2014) Mechanical assessment and deformation mechanisms of aluminum foam filled stainless steel braided tubes subjected to transverse loading, Thin Wall Struct 79:95-107.
[45] Yang S.Qi C (2013) Multiobjective optimization for empty and foam-filled square columns under oblique impact loading, Int J Impact Eng 54:177-191.
[46] Karagiozova D, Nurick G N.Chung Kim Yuen S (2005) Energy absorption of aluminium alloy circular and square tubes under an axial explosive load, 43:956 - 982.
[47] Liu S, Tong Z, Tang Z, Liu Y.Zhang Z (2015) Bionic design modification of non-convex multi-corner thin-walled columns for improving energy absorption through adding bulkheads, Thin Wall Struct 88:70-81.
[48] Duarte I, Vesenjak M, Krstulovi Opara L, An El I.Ferreira J M F (2015) Manufacturing and bending behaviour of in situ foam-filled aluminium alloy tubes, Mater Design 66:532-544.
[49] Lee K, Yang Y, Kim S.Yang I (2008) Energy absorption control characteristics of AL thin-walled tubes under impact load, Acta Mech Solida Sin 21:383-388.
[50] Zhang L, Bai Z.Bai F (2018) Crashworthiness design for bio-inspired multi-cell tubes with quadrilateral, hexagonal and octagonal sections, Thin Wall Struct 122:42-51.
[51] Chen W.Wierzbicki T (2001) Relative merits of single-cell, multi-cell and foam-filled thin-walled structures in energy absorption, Thin Wall Struct 39:287-306.